Lumped Parameter Outflow Models for 1-D Blood Flow Simulations: Effect on Pulse Waves and Parameter Estimation

J. Alastruey[1,2,*], K. H. Parker[2], J. Peiró[1] and S. J. Sherwin[1]

[1] *Department of Aeronautics, Imperial College London, South Kensington Campus, London SW7 2AZ, U.K.*
[2] *Department of Bioengineering, Imperial College London, South Kensington Campus, London SW7 2AZ, U.K.*

Abstract. Several lumped parameter, or zero-dimensional (0-D), models of the microcirculation are coupled in the time domain to the nonlinear, one-dimensional (1-D) equations of blood flow in large arteries. A linear analysis of the coupled system, together with *in vivo* observations, shows that: (i) an inflow resistance that matches the characteristic impedance of the terminal arteries is required to avoid non-physiological wave reflections; (ii) periodic mean pressures and flow distributions in large arteries depend on arterial and peripheral resistances, but not on the compliances and inertias of the system, which only affect instantaneous pressure and flow waveforms; (iii) peripheral inertias have a minor effect on pulse waveforms under normal conditions; and (iv) the time constant of the diastolic pressure decay is the same in any 1-D model artery, if viscous dissipation can be neglected in these arteries, and it depends on all the peripheral compliances and resistances of the system. Following this analysis, we propose an algorithm to accurately estimate peripheral resistances and compliances from *in vivo* data. This algorithm is verified against numerical data simulated using a 1-D model network of the 55 largest human arteries, in which the parameters of the peripheral windkessel outflow models are known *a priori*. Pressure and flow waveforms in the aorta and the first generation of bifurcations are reproduced with relative root-mean-square errors smaller than 3%.

AMS subject classifications: 92C35, 35L45

Key words: Pulse wave propagation, one-dimensional modelling, lumped parameter outflow models, time-domain coupling, arterial compliance, peripheral compliance, peripheral resistance, multiscale modelling.

*Corresponding author. *Email addresses:* `jordi.alastruey-arimon@imperial.ac.uk` (J. Alastruey), `k.parker@imperial.ac.uk` (K. H. Parker), `j.peiro@imperial.ac.uk` (J. Peiró), `s.sherwin@imperial.ac.uk` (S. J. Sherwin)

1   Introduction

Arterial pulse wavelengths are sufficiently long to mathematically justify the use of a one-dimensional (1-D) rather than a three-dimensional (3-D) approach when a global assessment of blood flow in the cardiovascular system is required. Several comparisons against *in vivo* [19, 26] and *in vitro* [2, 16] data have shown the ability of the nonlinear, 1-D equations of blood flow in compliant vessels [11, 14, 21, 23, 29] to capture the main features of pressure and flow waveforms in large arteries. These tests have increased our confidence in applying the 1-D formulation to clinically relevant problems [3–5, 13, 25, 26, 28] or to provide the boundary conditions for 3-D simulations [10]. However, the clinical relevance of 1-D modelling is subject to the availability of patient-specific data on the geometry, local pulse wave speeds, and boundary conditions of the arterial network to be simulated.

Recent progress in imaging technology has open greater possibilities for the application of 1-D modelling. Imaging techniques such as computer tomography, magnetic resonance and ultrasound are now able to provide patient-specific information on vessel geometry as well as more limited information on local velocity profiles and pulse wave speeds. This information permits the use of the 1-D formulation to simulate patient-specific arterial networks provided that appropriate boundary conditions are prescribed. Although the inflow waveform at the root of the arterial model (typically at the ascending aorta) can be accurately measured at salient locations using medical imaging, determination of outflow boundary conditions based on measured data is more challenging.

Even if such data were available, it is computationally too expensive to model all vessels in the full systemic circulation using the 1-D formulation because of their large number, which increases exponentially as more generations of the arterial tree are introduced. Furthermore, the assumptions of the 1-D equations become less appropriate with the decreasing caliber of the vessels. For instance, blood flow in large arteries is pulsatile and dominated by inertia, whereas blood flow in smaller vessels is quasi-steady and dominated by viscosity [7]. Consequently, any 1-D model has to be truncated after a relatively small number of generations of bifurcations, and the haemodynamic effect of vessels beyond 1-D model arteries is typically simulated using lumped parameter or zero-dimensional (0-D) models governed by ordinary differential equations that relate pressure to the flow at the outflow of each 1-D terminal vessel [3–5, 13, 25, 26, 28]. Alternatively, the remainder of the arterial system can be simulated using structured tree models based on Womersley's elastic vessel theory under the assumption of periodic flow [18, 19].

The aim of this investigation is to provide appropriate outflow 0-D models for patient-specific simulations and to propose a strategy to estimate their parameters using data that can be measured *in vivo*. Several physiologically relevant 0-D models are coupled to the nonlinear, 1-D formulation using a time-domain algorithm that can accommodate periodic and transient phenomena. The resulting 1-D/0-D multiscale formulation is linearized to study the main effects of 0-D outflow parameters on pulse wave propagation in 1-D model arteries, and to devise a strategy to select the parameters of the outflow mod-

els from available *in vivo* data that capture the main haemodynamic features of vessels beyond the arteries of the 1-D tree model and reduce artificial wave reflections. Numerical examples will show the suitability of the algorithms proposed.

2   Methodology

Sections 2.1 and 2.2 introduce the 1-D and 0-D formulations, respectively, and show the relation between their parameters and variables. Section 2.3 discusses how to couple both formulations in the time-domain and applies the coupling algorithm to physiologically relevant 0-D outflow models. Section 2.4 analyzes the effect of the parameters of the outflow models on waveform patterns using the linearized 1-D/0-D multiscale system. Section 2.5 suggests a strategy to estimate these parameters using data measurable *in vivo*.

2.1   1-D formulation

Conservation of mass and balance of momentum applied to a 1-D impermeable and deformable tubular control volume of Newtonian incompressible fluid yields a nonlinear system of partial differential equations that can be expressed in non-conservative form as [23]

$$
\frac{\partial \mathbf{U}}{\partial t} + \mathbf{H}\frac{\partial \mathbf{U}}{\partial x} = \mathbf{S},
$$

$$
\mathbf{U} = \begin{bmatrix} A \\ U \end{bmatrix}, \qquad \mathbf{H} = \begin{bmatrix} U & A \\ \frac{1}{\rho}\frac{\partial P}{\partial A} & U \end{bmatrix}, \qquad \mathbf{S} = \begin{bmatrix} 0 \\ \frac{1}{\rho}\left(\frac{f}{A} - s\right) \end{bmatrix},
$$

(2.1)

where x is the axial coordinate along the vessel, t is the time, $A(x,t)$ is the cross-sectional area of the lumen, $U(x,t)$ is the average axial velocity, $P(x,t)$ is the average internal pressure over the cross section, and $\rho = 1050$ Kg m^{-3} is the density of blood. The friction force per unit length f is given by [25, 29]

$$
f = 2\mu\pi\hat{R}\left[\frac{\partial u}{\partial r}\right]_{r=\hat{R}},
$$

where $\mu = 4$ mPa·s is the blood viscosity, $\hat{R}(x,t)$ is the lumen radius, $u(x,r,t)$ is the axial velocity (r is the radial coordinate). The source term s accounts for additional effects such as the action of gravity, the tapering of the vessel wall, and the nonlinearity of the sectional integration in terms of u. A typical profile for axisymmetric flow satisfying the no-slip condition is

$$
u = U\frac{\gamma+2}{\gamma}\left[1 - \left(\frac{r}{\hat{R}}\right)^{\gamma}\right],
$$

where γ is a constant [25,29], so that $f = -2(\gamma+2)\mu\pi U$. According to [25], $\gamma=9$ is a good compromise fit to the experimental data. Notice that $\gamma=2$ corresponds to a parabolic profile which leads to Poiseuille's flow resistance $f=-8\mu\pi U$.

Following previous works [2–5,11,13,18,19,23,26], we adopt a pressure-area relationship of the form

$$P = \frac{\beta}{A_0}\left(\sqrt{A} - \sqrt{A_0}\right), \qquad \beta(x) = \frac{4}{3}\sqrt{\pi}hE, \tag{2.2}$$

which assumes a thin, homogeneous, incompressible and elastic arterial wall, in which each section is independent of the others, with a thickness $h(x)$, a Young's modulus $E(x)$, and a lumen area $A_0(x)$ at the reference state $(P,U)=(0,0)$. In the presence of elastic and geometrical tapering of the arterial wall, the source term s in Eq. (2.1) is given by

$$s = \frac{\partial P}{\partial \beta}\frac{d\beta}{dx} - \frac{\partial P}{\partial A_0}\frac{dA_0}{dx}.$$

Under physiological conditions, $A>0$ and $\frac{1}{\rho}\frac{\partial P}{\partial A}>0$. Therefore, **H** has two real eigenvalues, $\lambda_{f,b}=U\pm c$, where

$$c = \sqrt{\frac{A}{\rho}\frac{\partial P}{\partial A}} = \sqrt{\frac{\beta}{2\rho A_0}}A^{1/4}$$

is the pulse wave speed and $U\ll c$. The system in (2.1) can be written in diagonal form as

$$\frac{\partial \mathbf{W}}{\partial t} + \mathbf{\Lambda}\frac{\partial \mathbf{W}}{\partial x} = \mathbf{S}_w, \tag{2.3}$$

with

$$\mathbf{W} = \begin{bmatrix} W_f \\ W_b \end{bmatrix}, \qquad \mathbf{\Lambda} = \begin{bmatrix} \lambda_f & 0 \\ 0 & \lambda_b \end{bmatrix}, \qquad \mathbf{S}_w = \begin{bmatrix} \frac{1}{\rho}\left(\frac{f}{A}-s\right) \\ \frac{1}{\rho}\left(\frac{f}{A}-s\right) \end{bmatrix},$$

where $W_{f,b}=U\pm4(c-c_0)$ are the characteristic or Riemann variables of the system, with $c_0=c(A_0)$. Eq. (2.3) shows that changes in pressure and velocity are propagated forward (in the positive direction of x) by W_f and backward (in the negative direction of x) by W_b along the characteristic curves

$$\frac{d}{dt}\hat{x}_{f,b} = \lambda_{f,b},$$

respectively, where $\hat{x}_{f,b} = \hat{x}_{f,b}(t)$ represent curves in the (x,t) space. Consequently, one boundary condition has to be prescribed at each side of the control volume. The source term $\mathbf{S}_w$ changes the values of W_f and W_b as they propagate.

We have previously solved system (2.1) with the tube law (2.2) in arterial networks using a discontinuous Galerkin scheme with a Legendre polynomial spectral/hp-spatial discretization and a second-order Adams-Bashforth time-integration scheme [2, 23], and we have validated this formulation against *in vitro* data [2, 16]. To simplify the analysis of the coupled 1-D/0-D model, a linear formulation is obtained as follows. Expressing

Eqs. (2.1) and (2.2) in terms of the (A,P,Q) variables, with $Q=AU$, and linearizing them about the reference state $(A_0,0,0)$, with β and A_0 constant along x, yields

$$\begin{cases} C_{1D}\dfrac{\partial p}{\partial t}+\dfrac{\partial q}{\partial x}=0, \\[2mm] L_{1D}\dfrac{\partial q}{\partial t}+\dfrac{\partial p}{\partial x}=-R_{1D}q, \\[2mm] p=\dfrac{a}{C_{1D}}, \end{cases} \tag{2.4}$$

where a, p and q are the perturbation variables for area, pressure and volume flux, respectively, i.e. $(A,P,Q)=(A_0+a,p,q)$, and

$$R_{1D}=\frac{2(\gamma+2)\pi\mu}{A_0^2}, \qquad L_{1D}=\frac{\rho}{A_0}, \qquad C_{1D}=\frac{A_0}{\rho c_0^2} \tag{2.5}$$

are the viscous resistance to flow, blood inertia and wall compliance, respectively, per unit of length of vessel. From Eq. (2.2) we have

$$\frac{\partial p}{\partial a}=\frac{\partial P}{\partial A}\bigg|_{A=A_0}=\frac{1}{C_{1D}}.$$

The method of characteristics shows that linear changes in pressure and volume flux are propagated forward by w_f at a speed c_0 and backward by w_b at a speed $-c_0$, given by

$$w_{f,b}=q\pm\frac{p}{Z_0}, \qquad Z_0=\frac{\rho c_0}{A_0}. \tag{2.6}$$

The flows w_f and w_b are the linear Riemann variables and Z_0 is the characteristic impedance of the vessel.

2.2 0-D formulation

Eq. (2.4) can be further simplified by integration along the length, l, of an arterial domain in which $x\in[0,l]$,

$$\begin{cases} C_{0D}\dfrac{\mathrm{d}\hat{p}}{\mathrm{d}t}+q_{out}-q_{in}=0, \\[2mm] L_{0D}\dfrac{\mathrm{d}\hat{q}}{\mathrm{d}t}+R_{0D}\hat{q}+p_{out}-p_{in}=0, \end{cases}$$

where $q_{in}(t)=q(0,t)$, $q_{out}(t)=q(l,t)$, $p_{in}(t)=p(0,t)$ and $p_{out}(t)=p(l,t)$ are the flows and pressures at the inlet and outlet of the domain, $R_{0D}=R_{1D}l$, $L_{0D}=L_{1D}l$, $C_{0D}=C_{1D}l$, and

$$\hat{p}(t)=\frac{1}{l}\int_0^l p\mathrm{d}x, \qquad \hat{q}(t)=\frac{1}{l}\int_0^l q\mathrm{d}x$$
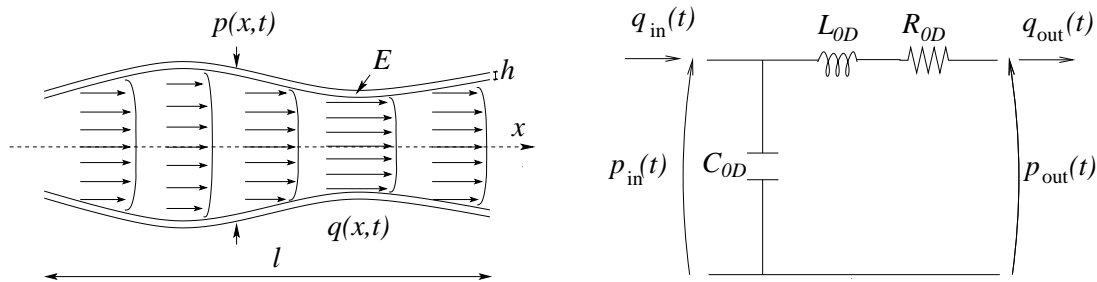
Figure 1: A finite number of 0-D systems (2.7) (right) discretize, at first order in space, a linear continuous 1-D arterial domain of length l governed by the system (2.4) (left).

are the mean pressure and flow over the whole domain. Milišić and Quarteroni [17] proved that if $\hat{p} = p_{in}$ and $\hat{q} = q_{out}$[†], so that

$$
\begin{cases}
C_{0D}\dfrac{dp_{in}}{dt} + q_{out} - q_{in} = 0, \\[2mm]
L_{0D}\dfrac{dq_{out}}{dt} + R_{0D}q_{out} + p_{out} - p_{in} = 0,
\end{cases}
\tag{2.7}
$$

then a finite number N of zero-dimensional (0-D) systems (2.7), each with length $\Delta x = l/N$, discretize, at first- order accuracy in space, a linear continuous 1-D arterial domain of length l governed by Eq. (2.4). This idea has been previously implemented to simulate pulse wave propagation in systemic human arteries [6,22,32].

Eq. (2.7) are analogous to the electric transmission line equations, in which the role of the flow and pressure are played by the electric current and potential, respectively, R_{0D} corresponds to an electric resistance, L_{0D} to an inductance, and C_{0D} to a capacitance (Fig. 1). Integration of Eq. (2.7) over a period of time $[t', t'+T]$ yields

$$
\begin{cases}
C_{0D}[p_{in}(t'+T) - p_{in}(t')] + T(\overline{q}_{out} - \overline{q}_{in}) = 0, \\[2mm]
L_{0D}[q_{out}(t'+T) - q_{out}(t')] + T(R_{0D}\overline{q}_{out} + \overline{p}_{out} - \overline{p}_{in}) = 0,
\end{cases}
\tag{2.8}
$$

where

$$
\overline{q}_{in} = \frac{1}{T}\int_{t'}^{t'+T} q_{in}\,dt, \quad \overline{p}_{in} = \frac{1}{T}\int_{t'}^{t'+T} p_{in}\,dt, \quad \overline{q}_{out} = \frac{1}{T}\int_{t'}^{t'+T} q_{out}\,dt, \quad \overline{p}_{out} = \frac{1}{T}\int_{t'}^{t'+T} p_{out}\,dt
$$

are the mean values of q_{in}, p_{in}, q_{out} and p_{out} over the interval $[t', t'+T]$, respectively. If the flow is periodic with a period T, Eq. (2.8) reduces to

$$
\overline{q}_{in} = \overline{q}_{out} = \frac{\overline{p}_{in} - \overline{p}_{out}}{R_{0D}}.
\tag{2.9}
$$

[†]The justification for this is that, under physiological conditions, pulse waves are much faster than blood velocity.

A 0-D approach is commonly used to simulate the perfusion of the micro-circulation and can account for other physiological processes such as flow auto-regulation by vasoconstriction and vasodilatation [3]. In general, a 0-D model can be described as a system of ordinary differential equations

$$\frac{d\mathbf{y}}{dt} = \mathbf{A}\mathbf{y} + \mathbf{b}(\mathbf{y},t), \tag{2.10}$$

where $\mathbf{y} \in \mathbb{R}^m$ is a vector of variables, $\mathbf{A} \in \mathbb{R}^{m \times m}$ is a matrix of parameters and $\mathbf{b} \in \mathbb{R}^m$ is a source term that provides external data to the system. In particular, Eq. (2.7) can be written as (2.10) with

$$\mathbf{y} = \begin{bmatrix} p_{in} \\ q_{out} \end{bmatrix}, \qquad \mathbf{A} = \begin{bmatrix} 0 & -\frac{1}{C_{0D}} \\ \frac{1}{L_{0D}} & -\frac{R_{0D}}{L_{0D}} \end{bmatrix}, \qquad \mathbf{b} = \begin{bmatrix} \frac{q_{in}}{C_{0D}} \\ -\frac{p_{out}}{L_{0D}} \end{bmatrix}.$$

2.3   Coupling 1-D and 0-D models

The existence and uniqueness of the solution of a coupled problem involving a 0-D model expressed in the form of Eq. (2.10) and the hyperbolic 1-D system (2.3), with $\mathbf{S}_w = \mathbf{0}$, has been proven in [9] for a sufficiently small time so that the characteristic curve leaving the 1-D/0-D interface does not intersect with incoming characteristic curves. Numerically, the coupling problem is established through the solution of a Riemann problem at the 1-D/0-D interface (Fig. 2, bottom left). An intermediate state (A^*,U^*) originates at time $t+\Delta t$ (Δt is the time step) from the states (A_L,U_L) and (A_R,U_R) at time t. The state (A_L,U_L) corresponds to the end point of the 1-D domain, and (A_R,U_R) is a virtual state selected so that (A^*,U^*) satisfies the relation between A^* and U^* dictated by Eq. (2.10). The 1-D and 0-D variables at the interface are related through

$$q_{in} = A^*U^*, \quad p_{in} = \frac{\beta}{A_0}\left(\sqrt{A^*} - \sqrt{A_0}\right),$$

and p_{out} is prescribed as a constant parameter that represents the pressure at which flow to the venous system ceases.

If $\mathbf{S}_w = \mathbf{0}$, Eq. (2.3) leads to

$$W_f(A^*,U^*) = W_f(A_L,U_L), \tag{2.11}$$
$$W_b(A^*,U^*) = W_b(A_R,U_R). \tag{2.12}$$

Solving Eqs. (2.11) and (2.12) for A^* and U^* yields

$$A^* = \left[\sqrt{\frac{2\rho A_0}{\beta}}\frac{W_f(A_L,U_L) - W_b(A_R,U_R)}{8} + A_0^{1/4}\right]^4, \tag{2.13}$$

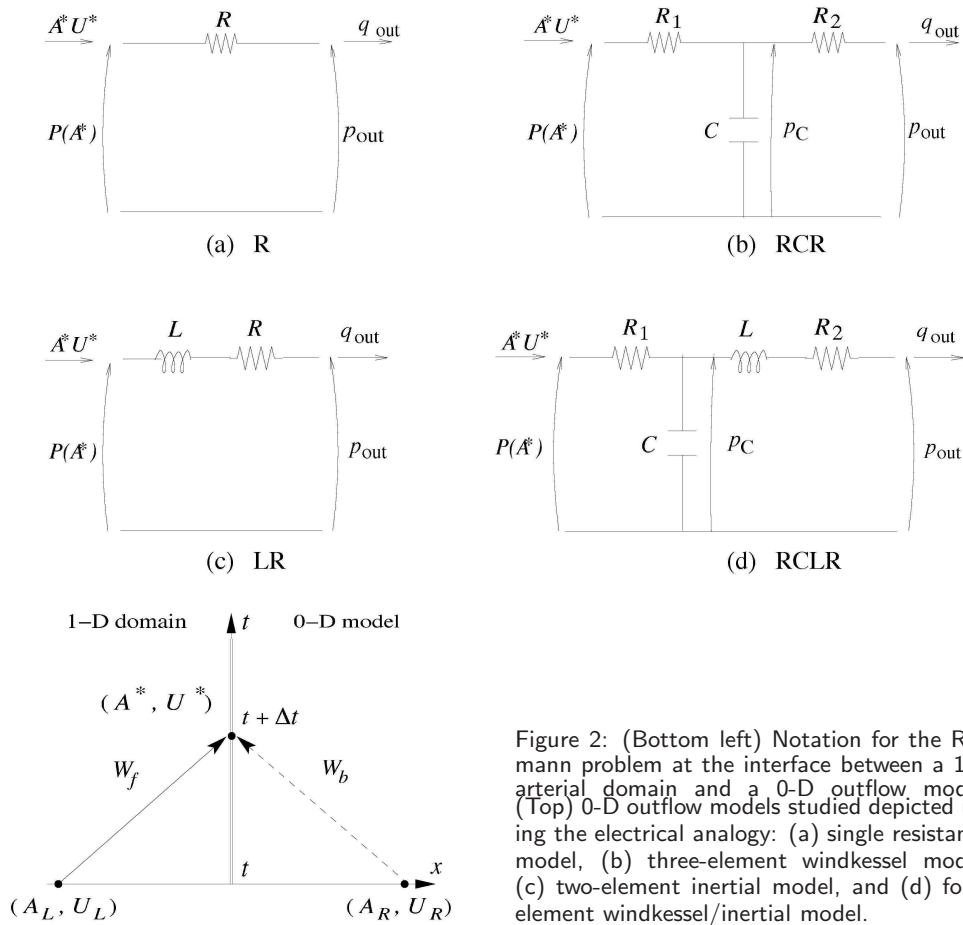$$U^* = \frac{1}{2}\left(W_f(A_L,U_L) + W_b(A_R,U_R)\right). \tag{2.14}$$

Figure 2: (Bottom left) Notation for the Riemann problem at the interface between a 1-D arterial domain and a 0-D outflow model. (Top) 0-D outflow models studied depicted using the electrical analogy: (a) single resistance model, (b) three-element windkessel model, (c) two-element inertial model, and (d) four-element windkessel/inertial model.

The 1-D outflow boundary condition is imposed by enforcing that either $U_R = U_L$, which reduces Eq. (2.13) to

$$A_R = \left[2(A^*)^{1/4} - (A_L)^{1/4} \right]^4, \tag{2.15}$$

or $A_R = A_L$, which reduces Eq. (2.14) to

$$U_R = 2U^* - U_L. \tag{2.16}$$

2.3.1   Physiologically relevant 0-D outflow models

The resistance, R, the compliance, C, and the fluid inertia, L, of vessels peripheral to a 1-D domain can be simulated using the four-element (RCLR) windkessel/inertial model shown in Fig. 2(d), with $R = R_1 + R_2$. The initial resistance, R_1, is introduced to absorb the incoming waves and reduce artificial wave reflections. It satisfies

$$A^* U^* = \frac{P(A^*) - (p_C)^n}{R_1}, \tag{2.17}$$

where $(p_C)^n$ is the pressure at C at the time step n. This choice of model will be justified in Section 2.4.1. The CLR_2 system is governed by Eq. (2.7), with $C_{0D} = C$, $L_{0D} = L$, $R_{0D} = R_2$, $p_{in} = p_C$ and $q_{in} = A^*U^*$. A first-order time discretization of Eq. (2.7) is written as

$$C\frac{(p_C)^n - (p_C)^{n-1}}{\Delta t} + (q_{out})^n - A^*U^* = 0, \tag{2.18}$$

$$L\frac{(q_{out})^n - (q_{out})^{n-1}}{\Delta t} + R_2(q_{out})^n + p_{out} - (p_C)^n = 0, \tag{2.19}$$

with $(p_C)^{n-1} = 0$ and $(q_{out})^{n-1} = 0$ for the initial time step, $n = 1$. Combining Eq. (2.18) and (2.19) yields

$$\phi(p_C)^n = \frac{R_2 C}{\Delta t}(p_C)^{n-1} + R_2 A^*U^* + \frac{R_2}{L + R_2\Delta t}\left[\Delta t p_{out} - L(q_{out})^{n-1}\right], \tag{2.20}$$

where

$$\phi = \frac{R_2 C}{\Delta t} + \frac{R_2\Delta t}{L + R_2\Delta t}.$$

Eq. (2.20) combines with (2.17) to produce

$$A^*U^* = \frac{P(A^*) - (p_{out})_{RCLR}}{R_1 + R_2/\phi}, \tag{2.21}$$

where

$$(p_{out})_{RCLR} = (p_C)^n - \frac{R_2}{\phi}A^*U^*.$$

Combining (2.21) and (2.11), and expressing $P(A^*)$ through the tube law (2.2) yields the nonlinear equation

$$\mathcal{F}(A^*) = \left(R_1 + \frac{R_2}{\phi}\right)\left(\left[U_L + 4c(A_L)\right]A^* - 4c(A^*)A^*\right)$$

$$- \frac{\beta}{A_0}\left(\sqrt{A^*} - \sqrt{A_0}\right) + (p_{out})_{RCLR} = 0, \tag{2.22}$$

that is solved using the Newton's method with the initial guess $A^* = A_L$. Once A^* has been obtained, U^* is calculated from (2.21) and the boundary condition is prescribed either through (2.15) or (2.16).

Note that if $L = 0$, we obtain the three-element windkessel model shown in Fig. 2(b). If $C = 0$, we obtain the two-element inertial model shown in Fig. 2(c). Finally, if both C and L are equal to zero, we recover a single resistance model, Fig. 2(a), in which Eq. (2.21) reduces to

$$A^*U^* = \frac{P(A^*) - p_{out}}{R}. \tag{2.23}$$

2.4 Effect of 0-D outflow models on 1-D waveforms

This section studies the effect of the parameters of the 0-D outflow models on the wave-forms propagated in an arterial network. Pulse wave propagation is simulated using the linear 1-D formulation, which makes the analysis simpler and its use is justified because the effect of nonlinearities is small under physiological conditions, as we have shown in [16]. The study is divided into analysis of the 'local' effect on a terminal 1-D domain and of the 'global' effect involving all the arterial domains of a 1-D network.

2.4.1 Local effect

If the linear 1-D formulation is used, Eq. (2.23) becomes $q^* = (p^* - p_{out})/R$. It can be expressed as a function of the linear Riemann variables (2.6) applying $q^* = (w_f + w_b)/2$ and $p^* = Z_0(w_f - w_b)/2$,

$$w_b = -R_t w_f - \frac{2p_{out}}{R + Z_0}, \qquad R_t = \frac{R - Z_0}{R + Z_0}, \qquad (2.24)$$

where R_t is the terminal reflection coefficient. A perturbation $(\delta p, \delta q)$ propagating in the forward direction of the 1-D domain; i.e., $w_b = 0$ and $\delta q = \delta p / Z_0$, produces a reflected state $(\delta p^*, \delta q^*)$ that satisfies $w_f(\delta p^*, \delta q^*) = w_f(\delta p, \delta q)$. Using Eq. (2.24) to relate $w_f(\delta p^*, \delta q^*)$ to $w_b(\delta p^*, \delta q^*)$ and transforming the Riemann variables into pressure and flow volume leads to

$$\delta p^* = (1 + R_t)\delta p + \frac{Z_0 p_{out}}{R + Z_0}, \qquad \delta q^* = (1 - R_t)\delta q - \frac{p_{out}}{R + Z_0}. \qquad (2.25)$$

Note that $R_t = 1$ (R tends to infinity) represents a closed end, in which the incoming pressure is doubled and the incoming velocity is annihilated ($\delta p^* = 2\delta p$, $\delta q^* = 0$)[‡], $R_t = -1$ ($R = 0$) corresponds to an open end with an outflow pressure p_{out}, in which the incoming pressure is annihilated and the incoming velocity is doubled ($\delta p^* = p_{out}$, $\delta q^* = 2\delta q - \frac{p_{out}}{Z_0}$), and $R_t = 0$ ($R = Z_0$) completely absorbs any incoming wave ($\delta p^* = \delta p + \frac{p_{out}}{2}$, $\delta q^* = \delta q - \frac{p_{out}}{2Z_0}$). Under physiological conditions, $R > Z_0$, so that $R_t > 0$.

If $C = 0$, Eq. (2.21) leads to the following relation between q^* and p^*

$$q^* = \frac{p^* - p_{out} + \frac{L}{\Delta t}(q_{out})^{n-1}}{R + \frac{L}{\Delta t}}, \qquad (2.26)$$

which shows that the inertial-resistance model produces reflected waves similar to the pure resistance model, but with a total resistance $R + L/\Delta t$ and a pressure gradient that depends on the inflow $(q_{out})^{n-1} = (q_{in})^{n-1}$. On the other hand, if $L = 0$ Eq. (2.21) yields

$$q^* = \frac{p^* - p_{out} + \frac{R_2 C}{\Delta t}((p_C)^n - (p_C)^{n-1})}{R}, \qquad (2.27)$$

[‡]Note that the reflected pressure is $\delta p^* - \delta p$ and the reflected flow is $\delta q^* - \delta q$.

where we have used $(p_C)^n = p^* - R_1 q^*$. Eq. (2.27) indicates that the RCR windkessel model can allow for more or less outflow q^* than the pure resistance model if the pressure at the compliance, p_C, is increasing or decreasing, respectively. Applying

$$q^* = \frac{w_f + w_b}{2}, \qquad p^* = Z_0 \frac{w_f - w_b}{2},$$

(2.27) is expressed in terms of the linear Riemann variables (2.6) as

$$w_b = -\Omega w_f - \frac{2[p_{out} + \frac{R_2 C}{\Delta t}(p_C)^{n-1}]}{R + Z_0 + \frac{R_2 C}{\Delta t}(R_1 + Z_0)}, \qquad \Omega = \frac{R - Z_0 + \frac{R_2 C}{\Delta t}(R_1 - Z_0)}{R + Z_0 + \frac{R_2 C}{\Delta t}(R_1 + Z_0)}. \tag{2.28}$$

The relation between a perturbation $(\delta p, \delta q)$ propagating in the forward direction of the 1-D domain and the corresponding reflected state $(\delta p^*, \delta q^*)$ is

$$\delta p^* = (1 + \Omega)\delta p + \frac{Z_0[p_{out} + \frac{R_2 C}{\Delta t}(p_C)^{n-1}]}{R + Z_0 + \frac{R_2 C}{\Delta t}(R_1 + Z_0)},$$

$$\delta q^* = (1 - \Omega)\delta q - \frac{p_{out} + \frac{R_2 C}{\Delta t}(p_C)^{n-1}}{R + Z_0 + \frac{R_2 C}{\Delta t}(R_1 + Z_0)}. \tag{2.29}$$

Note that when Δt tends to zero, Ω tends to $\frac{R_1 - Z_0}{R_1 + Z_0}$, which shows that $\Omega \delta p^*$ and $\Omega \delta q^*$ attain a minimum when $R_1 = Z_0$. Moreover, if $R_1 = 0$, Ω tends to -1 in the limit $\Delta t = 0$, which annihilates the incoming pressure and doubles the incoming flow.

2.4.2 Global effect

Applying Eq. (2.9) for each 1-D domain and 0-D outflow model (the latter with $R_{0D} = R$ and $\bar{p}_{out} = p_{out}$) of an arterial network with N domains and M outflows ($M < N$) shows that mean pressures and flow distributions in 1-D model arteries depend on the arterial, $(R_{0D})_i$ ($i = 1, \cdots, N$), and terminal, R_j ($j = 1, \cdots, M$), resistances of the system once a periodic state is reached, but not on the corresponding compliances, $(C_{0D})_i$ and C_j, and inertias, $(L_{0D})_i$ and L_j, which affect transient pressures and flows according to Eq. (2.8). Since the greatest fall in mean pressure occurs in the small arteries and arterioles in normal conditions [7], $(R_{0D})_i$ can be neglected compared to R_j, which leads to

$$\bar{q}_{IN} = \frac{\bar{p} - p_{out}}{R_T}, \qquad \frac{1}{R_T} = \sum_{j=1}^{M} \frac{1}{R_j}, \tag{2.30}$$

for a bifurcating network with M terminal domains, where $\bar{q}_{IN}$ is the mean inflow over a period T, $\bar{p}$ is the mean pressure in the N 1-D arterial domains, and R_T is the total resistance of the network. Furthermore, if $(L_{0D})_i$ ($i = 1, \cdots, N$) is also neglected and each outflow j ($j = 1, \cdots, M$) is simulated using a compliance C_j and resistance R_j, Eq. (2.7) leads to

$$\begin{cases} (C_{0D})_i \dfrac{\mathrm{d}(p_{in})_i}{\mathrm{d}t} + (q_{out})_i - (q_{in})_i = 0, \\ (p_{out})_i = (p_{in})_i = p, \end{cases} \tag{2.31}$$

for each arterial domain i ($i=1,\cdots,N$), where $p(t)$ is the pressure throughout the 1-D domains. Combination of (2.31) for each 1-D domain i ($i=1,\cdots,N$) with the peripheral resistances, R_j, and compliances, C_j ($j=1,\cdots,M$), leads to the windkessel model proposed by Frank [12], which lumps the arterial network into

$$C_T\frac{\mathrm{d}p}{\mathrm{d}t}+\frac{p-p_{out}}{R_T}-q_{IN}=0, \qquad C_T=\sum_{i=1}^{N}(C_{0D})_i+\sum_{j=1}^{M}C_j, \qquad (2.32)$$

where $q_{IN}(t)$ is the inflow flux volume and C_T is the total compliance calculated by adding the parallel arterial, $(C_{0D})_i$, and peripheral, C_j, compliances. Although Eq. (2.32) fails to reproduce the wave nature of pulse propagation because pressure changes are assumed to occur synchronously throughout the arteries, it is still applicable when wave activity is minimal. According to [1, 30] this is the case in approximately the last two thirds of diastole under normal conditions. During normal diastolic conditions $q_{IN}=0$ is a reasonable assumption that reduces Eq. (2.32) to

$$p-p_{out}=(p_0-p_{out})e^{\frac{-t}{R_T C_T}}, \qquad (2.33)$$

with p_0 the pressure at the start of diastole. Eq. (2.33) shows that the time constant $R_T C_T$ of the diastolic pressure decay is the same in any 1-D model artery, if viscous dissipation can be neglected in the 1-D model arteries, and it depends on all the peripheral compliances, C_j, and resistances, R_j ($j=1,\cdots,M$), of the system. The outflow pressure p_{out} affects both mean arterial pressures and flows and the diastolic part of arterial pulse waveforms.

2.5   Estimation of parameters of the 0-D model

The total resistance, R_T, of an arterial network can be calculated in two ways. It can be calculated using Eq. (2.30) if the inflow at the root of the network and a pressure measurement in any large artery are known, so that $\bar{q}_{IN}$ and $\bar{p}$ can be determined. Alternatively,

$$\frac{1}{R_T}=\sum_{j=1}^{M}\frac{1}{R_j}$$

can be used with $R_j=(\bar{p}-p_{out})/(\bar{q}_{out})_j$ if the mean outflow at each terminal vessel $(\bar{q}_{out})_j$ is available along with a pressure measurement in any large artery. Both techniques are valid provided that the flow can be assumed to be periodic and p_{out}, which takes a value of about 20 mmHg in normal conditions [7], is known. This pressure can be estimated together with the time constant $R_T C_T$ of the diastolic pressure decay by fitting Eq. (2.33) to a pressure waveform in any large artery [30]. In this case, flow periodicity is not required and long heart beats provide a more accurate fitting of p_{out} and $R_T C_T$, since wave activity decreases with time in each cardiac cycle. Once R_T is known, the total compliance, C_T, can be determined from the time constant $R_T C_T$.

The total peripheral compliance of the network can be calculated from Eq. (2.32) as

$$\sum_{j=1}^{M} C_j = C_T - \sum_{i=1}^{N} (C_{0D})_i.$$

According to Eq. (2.5), estimations of the geometry and pulse wave speeds are required to determine arterial compliances $(C_{0D})_i$. Arterial geometries can be reconstructed from image segmentation techniques and pulse wave speeds can be estimated using the PU-loop [15] or sum-of-the-squares [8] techniques. The value of the total peripheral compliance can be distributed in proportion to the flow distribution determined by the peripheral resistances R_j, as suggested in [28], or to the outflow cross-sectional areas.

Peripheral inertias can be neglected in normal conditions, as the numerical study in Section 3.1 will show.

In vivo data suggests that large arteries are well-matched for forward travelling waves [20, 31], so that peripheral reflected waves get 'trapped' as they propagate backwards toward the left ventricle. Furthermore, it has been shown that pulse waveforms in large arteries consist mainly of forward travelling waves [1, 30]. Therefore, the choice of an inflow resistance R_1 that matches the characteristic impedance of each of the terminal 1-D model arteries in order to minimize the intensity of the waves reflected by the windkessel models studied, and to avoid the generation of artificially reflected waves, seems to be justified.

3   Results and discussion

This section describes two simulations that provide supporting numerical evidence to the analysis presented in the previous sections. Section 3.1 considers the propagation of a narrow, Gaussian shaped input wave along a single artery connected to a 0-D model at the outflow and discusses the effect of the parameters of the 0-D model on the generated waveforms. The suitability of the method described in Section 2.5 for estimating the parameters of peripheral 0-D models is demonstrated using a 1-D model of the human arterial tree of known characteristics in Section 3.2.

3.1   Wave propagation in a single 1-D vessel coupled to several 0-D models

Fig. 3 shows the waveforms generated when a narrow, Gaussian shaped wave is propagated from the inlet of a single artery whose outlet is coupled to the 0-D models introduced in Section 2.3.1. A narrow, Gaussian shaped wave is a continuous approximation to the unit pulse $\delta(t)$ located at $t=0$ (i.e. $\delta(0)=1$ and $\delta(t)=0$ for $t\neq0$) used in [31] to track the multiple transmissions and reflections in the arterial system. The 1-D domain has a length $l=40$ cm, an initial lumen radius of 1 cm, a wall thickness $h=1.5$ mm and a Young's modulus $E=0.4$ MPa, based on the data published in [32] for the human aorta. The parameters of the 0-D models are $R=189$ MPa s m^{-3}, $C=6.3$ m^{3}GPa^{-1}, $L=1.0$ MKg
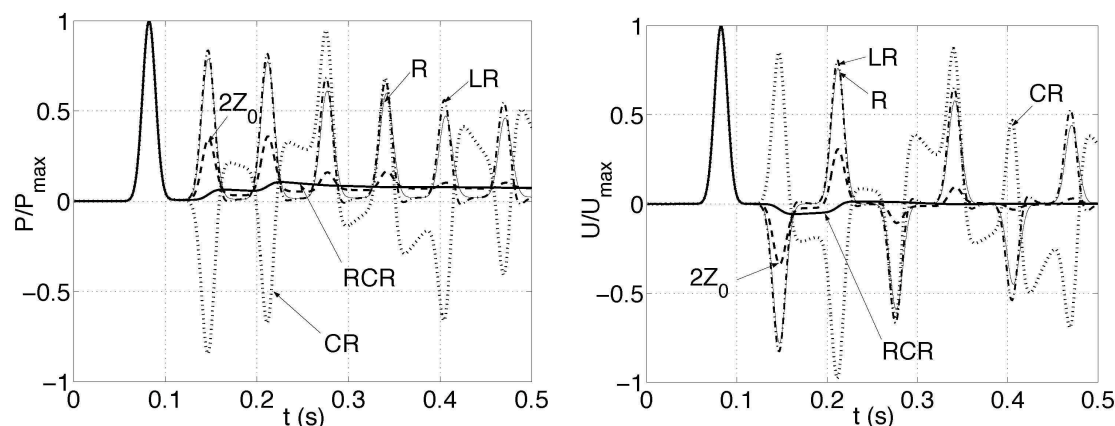
Figure 3: Propagation of a Gaussian shaped wave in the middle of a single 1-D arterial domain coupled to the following 0-D outflow models: single resistance (R), three-element windkessel with $R_1 = Z_0$ (RCR), $R_1 = 2Z_0$ ($2Z_0$) and $R_1 = 0$ (CR), and two-element inertial (LR) models. Pressure on the left and velocity on the right non-dimensionalized by their maximum values.

m^{-4} and $p_{out} = 0$. The values of R and C are based on data from [24], in which the aortic compliance, calculated as $C_{1D}l$ using (2.5) has been subtracted from the total compliance provided in [24]. The order of magnitude of L is that reported in [27] for the whole systemic circulation. Each simulation is run with 10 elements, using a polynomial of order 5 and a time step $\Delta t = 100 \ \mu$s.

The resistance (R) model produces reflected waves with pressure and velocity peaks of about 80% of their corresponding incident peaks, which is in agreement with the reflection coefficient $R_t = 0.8$ obtained from (2.24). Reflected waves maintain the sign of the incident waves in pressure but change it in velocity, in accordance to the linear reflections predicted by Eq. (2.25). Note that the inlet behaves as a closed end ($R_t = 1$), since the inflow is approximately zero by the time of arrival of the first reflected wave ($c_0 = 6.2$ m/s). The LR model produces similar reflected waves to the resistance model, but with an increase in their peaks of about 5%, which is in agreement with the behavior predicted by Eq. (2.26). Significant reflected waves are generated by the RCR model unless an initial resistance $R_1 = Z_0$ is used to match the propagation of forward travelling waves. The figure also shows the cases $R_1 = 2Z_0$ and $R_1 = 0$ (CR model). Note that the CR model produces negative reflected pressures and positive reflected velocities similar to the wave reflections generated by a single resistance model with $R_t = -0.8$. Finally, the pressure and velocity waves reflected by the matched RCLR model (i.e., $R_1 = Z_0$) cannot be distinguished in the scale of the figure from the corresponding waves reflected by the matched RCR model, which suggests that peripheral inertias have a minor effect on reflected waves under normal conditions.

Fig. 4 shows the waveforms obtained when a periodic half-sinusoidal inflow is imposed and $p_{out} = 1.33$ kPa. Once a quasi-steady state is reached, the matched RCR model is able to capture some features of *in vivo* aortic measurements [7], such as the pressure di-
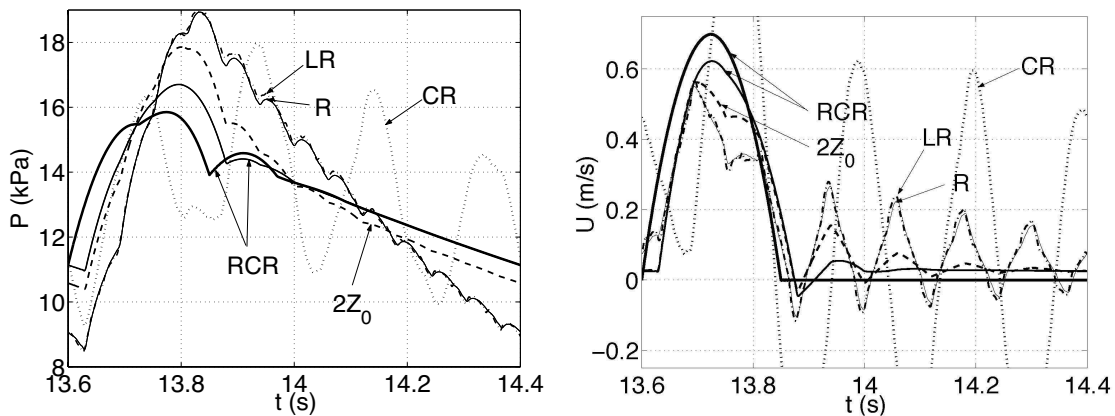
Figure 4: Pressure (left) and velocity (right) waveforms, once a quasi-steady state is reached, in the middle of a 1-D domain coupled to the 0-D outflow models as indicated in Fig. 3. A periodic half-sinusoidal flow rate with a mean flow of 3.8 l/min [24] is prescribed at the inlet. Waveforms are also shown at the inlet for the RCR model with $R_1 = Z_0$.

crotic notch, the exponential diastolic decay predicted by Eq. (2.33), the increase in pulse pressure towards the outlet, and some reversal flow at the end of systole. The matched RCLR model produces very similar results to the matched RCR model that cannot be distinguished in the scale of Fig. 4. The R, LR, RCR with $R_1 = 2Z_0$ and CR ($R_1 = 0$) models produce less physiological waveforms because they generate larger reflected waves (Fig. 3). These results suggest that peripheral vessels in arterial networks should be simulated using matched RCR models in normal physiological conditions. Resistance models can be applied if the total compliance C_T is mainly located in the 1-D model arteries, so that the system does not require any peripheral compliance to capture the correct time constant, $R_T C_T$, of the diastolic decay in Eq. (2.33). Note that mean pressures are the same in each simulation, which is in agreement with (2.30).

3.2 Wave propagation in a model of the 55 larger systemic arteries in the human

Fig. 6 shows two aortic pressure and flow waveforms simulated using the 1-D model of the 55 larger systemic arteries in the human proposed in [28] (Fig. 5). If terminal branches are coupled to matched RCR lumped parameter models, the system is able to capture the main features of aortic *in vivo* measurements discussed in Section 3.1. All the parameters of this simulation, which is referred to as the 'control case', are based on data provided in [28].

If resistance outflow models are used, pulse pressures increase by about 30% since the total compliance C_T of the system is reduced according to (2.32), which decreases the time constant in (2.33) and, as a result, the diastolic decay is steeper. However, mean pressures and flows remain unchanged once a quasi-steady state is reached, which is in agreement with (2.30). Single resistance models produce waveforms more similar to matched RCR

models in the 55 artery model than in the single 1-D model aorta shown in Fig. 4, since peripheral perfusion becomes more resistance and less compliant as more generations of bifurcations are simulated.
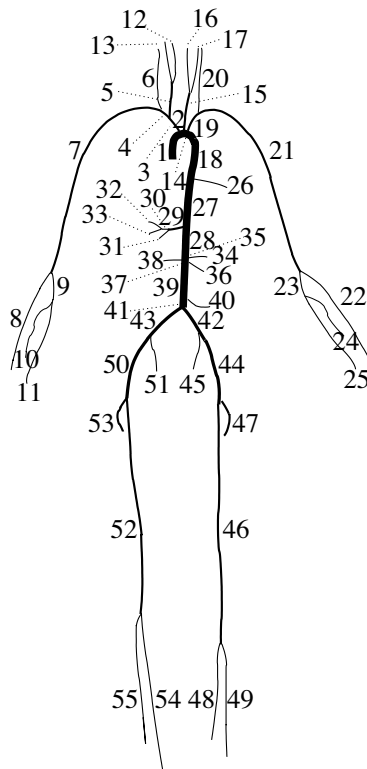

Figure 5: Connectivity of the 55 larger systemic arteries in the human, as proposed in [28].

Fig. 6 also shows the effect of lumping arteries beyond the first generation of bifurcations into matched RCR outflow models. If the new peripheral resistances and compliances are calculated by adding the R_{0D} and C_{0D} of the 1-D arterial segments beyond the first generation of bifurcations to the corresponding peripheral values, the root-mean-square errors in pressure and flow waveforms in the middle point of the aortic and first generation segments, relative to the corresponding maximum control values, are smaller than 3%. These errors are also smaller than 3% if the new peripheral resistances are estimated from the mean pressure in the middle point of segment 27 (thoracic aorta) and the mean flows in the middle points of the first generation of bifurcations, and the new peripheral compliances and outflow pressure p_{out} are determined by fitting Eq. (2.33) to the pressure waveform in the middle point of segment 27, as suggested in Section 2.5. The value of the total peripheral compliance is distributed in proportion to the outflow cross-sectional areas. These results suggest that matched RCR outflow models with adequately estimated parameters are able to accurately simulate the haemodynamic effect of peripheral compliant vessels on wave propagation in large arteries.
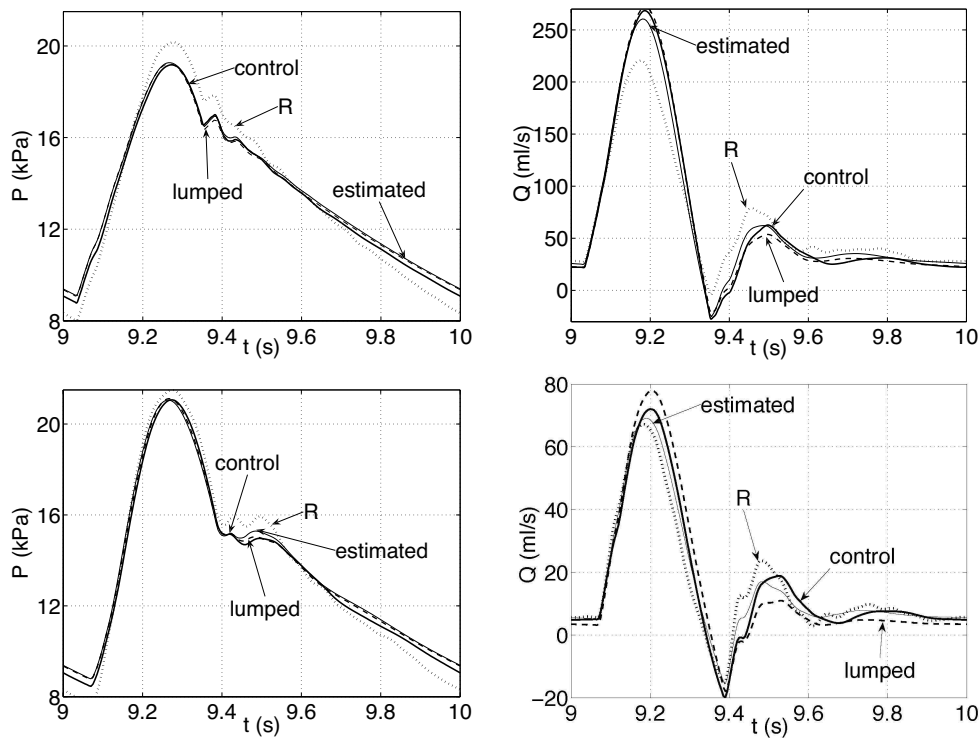
Figure 6: Pressure (left) and flow (right) waveforms in the middle of the aortic segments 27 (top) and 41 (bottom) as shown in Fig. 5. Terminal arteries coupled to matched RCR (control) and resistance (R) outflow models using the peripheral values in [28]. The corresponding waveforms obtained by lumping arteries beyond the first generation of bifurcations into matched RCR models are also shown, with peripheral resistances and compliances obtained by (i) adding the R_{0D} and C_{0D} of the 1-D arterial segments beyond the first generation of bifurcations to the corresponding peripheral values (lumped), and (ii) estimating their values as described in the text (estimated).

4 Conclusions

We have proposed a numerical algorithm to couple, in the time domain, nonlinear 1-D models for pulsatile blood flow in large arteries to 0-D models of the perfusion of the micro-circulation. The methodology presented highlights the reciprocal interaction between 1-D and 0-D models, and possesses good numerical convergence and stability properties. Different physiologically relevant 0-D outflow models have been implemented and the effect of their parameters on waveform patterns in large arteries has been studied. The coupling technique proposed permits the simulation of transient phenomena, which is required in some clinical applications, such as the study of the effect of sudden carotid occlusions on cerebral blood flows [3].

A linear analysis of the 1-D/0-D system in the time domain has allowed us to identify the effects of the parameters of the outflow 0-D models on arterial pulse waveforms, and to estimate their values using data that can be measured *in vivo*. In particular, we

have shown that mean pressures and flow distributions in large arteries depend on the resistances of the system once a periodic state is reached, but not on its compliances and inertias, which affect instantaneous pressure and flow waveforms. Peripheral inertias have a minor effect on flow waveforms under normal conditions. The time constant of the diastolic pressure decay is the same in any 1-D model artery, if viscous dissipation can be neglected in these arteries, and it depends on all the peripheral compliances and resistances of the system. Moreover, a lumped parameter windkessel model reduces artificial wave reflections if it contains an inflow resistance equal to the characteristic impedance of the 1-D domain. Finally, the main haemodynamic effects of peripheral vessels on pressure and flow wave propagation in the aorta and the first generation of bifurcations can be efficiently captured using a matched three-element windkessel model with peripheral resistances and compliances and outflow pressures estimated using the algorithm proposed in this work.

The results presented emphasize the significant influence of outflow models on 1-D flow simulations and the need for accurate estimation of their parameters in patient-specific simulations. Although this investigation is based on the linear 1-D equations and the results have only been tested using numerical data, it still offers important physiological insights into the haemodynamics of the vascular system, since the 1-D equations are able to capture the main features of pulse waveforms in large arteries [2, 16, 19, 26] and the effect of nonlinearities is small under physiological conditions [16]. Despite the growing interest in 3-D simulations in anatomically accurate geometries, the large range of scales within the human circulation implies that a combination of 3-D and 1-D models will be required for accurate, patient-specific modelling, as advocated in [10]. Moreover, the long length scales of pulse waves in large human systemic arteries compared to the characteristic arterial diameters suggests that the strength of the coupling of 3-D and 1-D models will be relatively small, thereby supporting an independent study of the 1-D/0-D reduced system. Future research will focus on showing the applicability of these results to *in vivo* data.

Acknowledgments

References

[1] J. Aguado-Sierra, J. Alastruey, J.J. Wang, N. Hadjiloizou, J.E. Davies, and K.H. Parker. Separation of the reservoir and wave pressure and velocity from measurements at an arbitrary location in arteries. *Accepted to Proceedings of the Institution of Mechanical Engineers, Part H, Journal of Engineering in Medicine*, 2007.

[2] J. Alastruey. *Numerical Modelling of Pulse Wave Propagation in the Cardiovascular System: Development, Validation and Clinical Applications*. PhD thesis, Imperial College London, University of London, 2006.

[3] J. Alastruey, S.M. Moore, K.H. Parker, T. David, J. Peiró, and S.J. Sherwin. Reduced modelling of blood flow in the cerebral circulation: Coupling 1-D, 0-D and cerebral auto-regulation models. *Int. J. Numer. Meth. Fluids*, 56:1061–1067, 2008.

[4] J. Alastruey, K.H. Parker, J. Peiró, S.M. Byrd, and S.J. Sherwin. Modelling the circle of Willis to assess the effects of anatomical variations and occlusions on cerebral flows. *J. Biomech.*, 40:1794–1805, 2007.

[5] J. Alastruey, K.H. Parker, J. Peiró, and S.J. Sherwin. Can the modified Allen's test always detect sufficient collateral flow in the hand? A computational study. *Comp. Meths. Biomech. Biomed. Engng.*, 9(6):353–361, 2006.

[6] A.P. Avolio. Multi-branched model of the human arterial system. *Med. and Biol. Engng. and Comput.*, 18:709–718, 1980.

[7] C.G. Caro, T.J. Pedley, R.C. Schroter, and W.A. Seed. *The Mechanics of the Circulation*. Oxford University Press, 1978.

[8] J.E. Davies, Z.I. Whinnett, D.P. Francis, K. Willson, R.A. Foale, I.S. Malik, A.D. Hughes, K.H. Parker, and J. Mayet. Use of simultaneous pressure and velocity measurements to estimate arterial wave speed at a single site in humans. *Am. J. Physiol. Heart Circ. Physiol*, 290:H878–H885, 2006.

[9] M.A. Fernández, V. Milišić, and A. Quarteroni. Analysis of a geometrical multiscale blood flow model based on the coupling of ODE's and hyperbolic PDE's. *SIAM J. Multiscale Mod. Sim.*, 4:215–236, 2005.

[10] L. Formaggia, J.F. Gerbeau, F. Nobile, and A. Quarteroni. On the coupling of 3D and 1D Navier-Stokes equations for flow problems in compliant vessels. *Comp. Meth. App. Mech. Engng.*, 191:561–582, 2001.

[11] L. Formaggia, D. Lamponi, and A. Quarteroni. One-dimensional models for blood flow in arteries. *J. Engng. Math.*, 47:251–276, 2003.

[12] O. Frank. Die Grundform des Arteriellen Pulses. *Z. Biol.*, 37:483–526, 1899.

[13] V.E. Franke, K.H. Parker, L.Y. Wee, N.M. Fisk, and S.J. Sherwin. Time domain computational modelling of 1D arterial networks in monochorionic placentas. *Mathem. Mod. and Num. Analysis*, 37:557–580, 2003.

[14] T.J.R. Hughes and J. Lubliner. On the one-dimensional theory of blood flow in larger vessels. *Math. Biosciences*, 18:161–170, 1973.

[15] A.W. Khir, A. O'Brien, J.S.R Gibbs, and K.H. Parker. Determination of wave speed and wave separation in the arteries. *J. Biomech.*, 34:1145–1155, 2001.

[16] K.S. Matthys, J. Alastruey, J. Peiró, A.W. Khir, P. Segers, P.R. Verdonck, K.H. Parker, and S.J. Sherwin. Pulse wave propagation in a model human arterial network: Assessment of 1-D numerical simulations against in vitro measurements. *J. Biomech.*, 40:3476–3486, 2007.

[17] V. Milišić and A. Quarteroni. Analysis of lumped parameter models for blood flow simulations and their relation with 1D models. *Mathem. Mod. and Num. Analysis*, 38:613–632, 2004.

[18] M.S. Olufsen. Structured tree outflow condition for blood flow in larger systemic arteries. *Am. J. Physiol.*, 276:H257–H268, 1999.

[19] M.S. Olufsen, C.S. Peskin, W.Y. Kim, E.M. Pedersen, A. Nadim, and J. Larsen. Numerical simulation and experimental validation of blood flow in arteries with structured-tree outflow conditions. *Annals Biomed. Engng.*, 28:1281–1299, 2000.

[20] G.L. Papageorgiou and N.B. Jones. Arterial system configuration and wave reflection. *J. Biomed. Engng.*, 9:299–301, 1987.

[21] T.J. Pedley. *The Fluid Mechanics of Large Blood Vessels*. Cambridge University Press, 1980.

[22] P. Segers and P. Verdonck. Role of tapering in aortic wave reflection: hydraulic and mathematical model study. *J. Biomech.*, 33:299–306, 2000.

[23] S.J. Sherwin, V.E. Franke, J. Peiró, and K.H. Parker. One-dimensional modelling of a vascular network in space-time variables. *J. Engng. Maths.*, 47:217–250, 2003.

[24] A.C. Simon, M.E. Safar, J.A. Levenson, G.M. London, B.I. Levy, and N.P. Chau. An evaluation of large arteries compliance in man. *Am. J. Physiol.*, 237:H550–H554, 1979.

[25] N.P. Smith, A.J. Pullan, and P.J. Hunter. An anatomically based model of transient coronary blood flow in the heart. *SIAM J. Appl. Math.*, 62:990–1018, 2001.

[26] B.N. Steele, J. Wan, J.P. Ku, T.J.R. Hughes, and C.A. Taylor. *In vivo* validation of a one-dimensional finite-element method for predicting blood flow in cardiovascular bypass grafts. *IEEE Trans. Biomed. Engng.*, 50:649–656, 2003.

[27] N. Stergiopulos, B.E. Westerhof, and N. Westerhof. Total arterial inertance as the fourth element of the windkessel model. *Am. J. Physiol.*, 45:H81–H88, 1999.

[28] N. Stergiopulos, D.F. Young, and T.R. Rogge. Computer simulation of arterial flow with applications to arterial and aortic stenoses. *J. Biomech.*, 25:1477–1488, 1992.

[29] S. Čanić and E.H. Kim. Mathematical analysis of the quasilinear effects in a hyperbolic model blood flow through compliant axi-symmetric vessels. *Math. Meth. Appl. Sci.*, 26:1161–1186, 2003.

[30] J.J. Wang, A.B. O'Brien, N.G. Shrive, K.H. Parker, and J.V. Tyberg. Time-domain representation of ventricular-arterial coupling as a windkessel and wave system. *Am. J. Heart Circ. Physiol.*, 284:H1358–H1368, 2003.

[31] J.J. Wang and K.H. Parker. Wave propagation in a model of the arterial circulation. *J. Biomech.*, 37:457–470, 2004.

[32] N. Westerhof, F. Bosman, C.J. de Vries, and A. Noordergraaf. Analog studies of the human systemic arterial tree. *J. Biomech.*, 2:121–143, 1969.